Experimentally Verifiable Modeling of Coplanar Waveguide Discontinuities

Vesna Radišić, Dag R. Hjelme, Aileen Horrigan, Zoya Basta Popović, and Alan R. Mickelson

Abstract— **A general technique for obtaining the frequency-dependent scattering parameters of open waveguiding structures is discussed. The first step of the analysis is an iterative solution for the charge distribution on the electrodes which, in our case, uses the "straight line" solution, the one first derived by Maxwell, as the starting value. A calibrated optical sampling technique allows for direct verification of the validity of the quasi-static charge distribution for structures in which the dielectric layers are also electrooptic. (Common waveguiding dielectrics such as GaAs and InP are sufficiently electrooptic to yield more than sufficient signal-to-noise ratios for accurate verification.) In cases where the quasi-static solution is valid, it is shown that the full dynamics of the propagation problem can be recovered from an equivalent nonuniform transmission line, the parameters of which can be determined from the phase velocity and impedance distribution defined by the static charge distribution. Here, we present analysis of planar discontinuities in coplanar waveguides (CPW), but the method can be modified and applied to include active devices, as well as three-dimensional discontinuities, such as airbridges. The method is based on an iterative solution of the quasi-static charge distribution using successive over relaxation and the dynamics are introduced via the Riccati equation. Additional measurements performed on the "in-house" fabricated passive circuits using an HP8510 Network Analyzer verify the accuracy of the dynamical part of the method.**

I. Introduction

ALTHOUGH TRANSMISSION line-models of open waveguide circuits can be quite efficacious, in many circumstances, real circuits with discontinuous and (possibly) closely spaced lines will also exhibit parasitics and line-to-line coupling, and in such cases, transmission line models break down. The parasitic effect is really caused by interaction of charge accumulations (largest near charge singularity points), which affect the continuous Maxwell charge distribution along the line. Coupling greatly complicates circuit equivalents of passive lines, while perturbations to charge distribution affect circuit values. An example of an unexpected result is that of a double stub tuner [1]. In such a case, however, it appears a circuit equivalent is available [2]. It is not at all clear that circuit equivalents even exist in stripline configurations which do not exhibit strict reciprocity.

Manuscript received September 20, 1992: revised February 1, 1993. This work was supported in part by the NSF Industry, the University Cooperative Research Center for Microwave/Millimeter Wave Computer-Aided Design under Grant CDR-8722832, and by the Office of Naval Research under Grant ONRN0014-92-J-1190. The work of A. Horrigan was supported in part by the Hughes Aircraft Fellowship.

The authors are with the Department of Electrical and Computer Engineering, University of Colorado, Boulder, CO 80309-0425.

IEEE Log Number 9211844.

Circuits that one practically wishes to consider usually contain active elements. In order for active elements to function at microwave frequencies, their dimensions must be small compared to the wavelength. The linewidths of the interconnections of stripline circuits are generally made to conform to the 50 Ω requirement and further to allow one to couple on and off the substrate. Microstrip lines must, therefore, be of the order of tens of microns. Although coplanar lines can scale and have impedances almost independent of substrate thickness, coupling requirements generally dictate characteristic dimensions of tens of microns. Due to limited carrier mobilities, the dimension of a transistor gate length is on the order of fractions of a micron. Total gate widths and, therefore, total device lengths are limited to tens (at most hundreds) of microns. Compactness requires that the external passive transmission lines taper rapidly down to the (sub) micron gate lengths. The typical dimensions for a parasitic coupling length is determined by some number of linewidths (one or two) of the passive line. One can conclude from these previously described considerations, that an active element is quite generally strongly parasitically coupled to its feedlines, and therefore its behavior (both linear and nonlinear) will be strongly dependent on the details of the local metallization.

Commercial software available at present, generally includes parasitics using transmission-line circuit models in conjunction with various discontinuous junction modes that can be inserted into the transmission lines (see, for example, the operating manual for HP's Microwave Design System). Such software packages generally include active elements through fitting the S-parameters to an assumed circuit model of a given complexity (which could include nonlinear circuit effects) and using this model in an overall circuit model of the system. Such models are phenomenological and can depend only weakly on the details of device geometry through the complex functions (S-parameters) determined for a given set of bias conditions. There also exist physics based programs which treat in detail the geometries and doping levels of each of the internal layers of the active region [3], [4]. Many of these models are restricted to two dimensions due to excessive run times. Even those which can run truly 3-D geometry have problems including the metallization layers. Neither ohmic nor Schottky barrier contacts, although commonly in use for decades, are well understood in terms of their effects on electron streams. If the effect of coupling the internal electron and hole streams is taken into account at all in a physical model, it is generally done by including multiple fitting parameters to fit to a given set of measured S-parameters [4].

Again, the details of the all-important parasitic couplings due to the details of the metallization are completely lost in this process.

There are really two problems hindering progress in the parasitic modeling area. One relates to the long computer time necessary to run either full wave models or physical charge flow models. Although it is generally argued that computer cycle times will decrease ad infinitum and therefore floating point operations per second will increase infinitely in the future, there is a competing effect. This effect is related to the restrictive assumptions that already go into the "exact" modeling techniques. There is a tendency for one to ever lift limitations on metallization thickness, current producing geometries, etc. as more computer power becomes available. Increased program complexity tends to offset increased run speed. It is not clear what happens to the ultimate predictability of physical effects.

A second hindrance to progress in the parasitic modeling arena has to do with the incompatibility of full wave analysis with physical modeling of the solid state effects. Above and beyond the complexity of modeling of ohmics and Schottkeys is the problem of trying to use a full wave approach for only a portion of a fully coupled region. Maxwell's equations cannot be solved exactly in such a case. One needs shields to separate the space into distinct regions or to model the whole of the coupled space. The physical device models suffer deficiencies on the other side. These models calculate charge transport and the local current and voltage effects induced by the transport. Such analysis ignores totally the effects of external dc and ac fields induced by parasitics and partially shielded by complicated metallization and doping distributions.

In this paper, we present a numerically efficient model which holds the promise for being eventually capable of taking parasitics into account in active circuits. The present work concentrates on quasi-static models of coplanar waveguide (CPW) structures. The goal is to develop a model which is stepwise experimentally verifiable, and can be used to propagate an electromagnetic disturbance through a CPW structure. In a future work, we plan to include active devices through phenomenological models which have been determined from optical sampling and HP8510 measurements used in concert with this numerically efficient algorithm.

There are many computer aided design (CAD) tools available for analysis of microstrip circuits. One quasi-static technique for analysis of microstrip circuits is presented in {5]. In general, quasi-static techniques should be n times faster than full wave techniques, where n is the number of frequency points, if both techniques are optimized. Quasi-static techniques are valid up to a certain frequency and this frequency limit depends on the type of the coplanar structure and its geometry. For CPW, the characteristic impedance and effective dielectric constant depend on the ratio of the widths of the inner conductor and the gaps and are almost independent of the substrate thickness. Therefore, the transverse dimensions of a CPW can be chosen to be very small compared to the wavelength. The quasi-static analysis of CPW structures should be valid even for very high frequencies. CPW offers several other advantages over conventional microstrip lines: it facilitates easy integration of shunt and series circuit elements, and it eliminates yield limiting backside processing, such as wafer thinning and via etching. These advantages make CPW well suited for monolithic microwave integrated circuits (MMICs), even though their application to present has been rather limited. This is partly due to a lack of CAD tools for CPW circuits, as compared with the tools available for analysis of microstrip circuits. Furthermore, little information is available in the literature on discontinuity models for CPW [6]. Even though there are an increasing number of characterization techniques becoming available [7]–[9], most of these are based on full-wave analysis which require large amounts of computer time and memory. Therefore, further development of simple and accurate modeling tools for CPW discontinuities is necessary.

The most common experimental verification of the quasi-static or full wave techniques is based on the use of a network analyzer. However, such measurements can yield only terminal characteristics, giving S-parameters after proper deembedding. Direct electrooptic sampling [12] can provide much more detailed information than network analyzer measurements can alone. Recent advances in electrooptic sampling allow one to obtain accurate 2-D potential distributions on planar microwave circuits [13].

The analysis technique presented in this paper was motivated by the 2-D electrooptic sampling measurements presented in [13]. Since our technique uses the 2-D potential distribution to compute the 2-D charge distribution, direct electrooptic probing seems to be an ideal tool to use as a verification of our analysis. The 2-D quasi-static charge distribution on the discontinuous transmission line is then transformed into an equivalent nonuniform transmission line. Since the quasi-static current distribution has zero divergence, a unique local coordinate system on the center conductor can be defined from the current field lines and their normals [5]. This defines a curvilinear coordinate system of the equivalent transmission line. The transmission line parameters are then expressed in terms of the static charge distribution. The propagation along the equivalent transmission line, therefore, recovers the full dynamics of the scattering problem from the static charge distribution. As the transmission-line problem is a one-dimensional one, the increase in the computation time due to this step is negligible compared to the quasi-static solution.

In problems involving waveguiding structures, there are two natural length scales: the wavelength of the radiation and the size of the guide. At microwave frequencies, the strip width of the internal conductors of the guide is generally much smaller than the wavelength of the guided radiation. Where this is not the case, the structure could act more as a radiating structure than as a waveguide. In our case the fields can be well described by a static field analysis [10]. Further, in the case of an ideal structure, the charge distribution of approximately static charges is well known from the early work of Maxwell [11]. Therefore, our analysis starts from an assumed or measured 2-D potential distribution on the center conductor and the ground planes of the circuit. Using a static Green's function, the surface charge distribution is found from this potential. The corresponding capacitance is

then calculated by integrating the charge distribution over the surface of the inner conductor. For any line that can be considered as a transmission line, knowledge of either the capacitance or inductance is sufficient for computing all line parameters including phase velocity and line impedance.

II. The Quasi-Static Approximation

The field solution to the discontinuity scattering problem possesses two scales. Near the discontinuity, the fields vary rapidly on a scale w, where w is the largest transverse dimension of the connecting lines, and then vary slowly with an $O(\lambda)$ scale, where λ is the free space wavelength of the exciting radiation, away from the discontinuity. The presence of these multiple scales can be used to derive an accurate approximations to the full wave problem [14].

A. A Multiple Scale Expansion

To perform a multiple scale expansion of Maxwell's equations, we introduce two scaled coordinates

$$\vec{r'} = \vec{r}/w \tag{1}$$

$$\vec{r''} = \vec{r}k \tag{2}$$

where $k = 2\pi/\lambda_{\text{eff}}$, and λ_{eff} is the effective wavelength on the transmission line. Introducing an expansion parameter

$$\alpha = kw \tag{3}$$

we can expand the electric field as [14]

$$E(r) = E^{(0)}(r', r'') + \alpha E^{(1)}(r', r'') + \alpha^2 E^{(2)}(r', r'') + \cdots . \tag{4}$$

A similar expansion is used for the magnetic field. The del-operator can be written as

$$\nabla = \frac{k}{\alpha}\left[\nabla' + \alpha \nabla''\right] \tag{5}$$

where the primed and double primed operators operate on r' and r'', respectively. Introducing the scaled coordinates and field expansions into Maxwell's equations and collecting orders of α, we obtain a multiple scale expansion of the field equations. The 0th-order terms (α^0) show that $E^{(0)}$ and $H^{(0)}$ satisfy the static Maxwell equations in the coordinate r'.

By introducing a new curvilinear coordinate system defined by the static field lines, and neglecting all longitudinal field components in this coordinate system, the first-order terms (α^1) show that $E^{(0)}$ and $H^{(0)}$ satisfy the source free Maxwell equations in the coordinate r''. These equations can be written as

$$\frac{\partial}{\partial u_3}\left(h_1 E_1^{(0)}\right) = i\frac{\omega\mu}{k} h_3 h_1 H_2^{(0)} \tag{6}$$

$$\frac{\partial}{\partial u_3}\left(h_2 H_2^{(0)}\right) = i\frac{\omega\epsilon}{k} h_3 h_2 E_1^{(0)} \tag{7}$$

where h_i are the metric coefficients of the curvilinear coordinate system u_i. The coordinate system is chosen such that $\vec{E}^{(0)}$ is tangential to $\vec{a}_1$ and $\vec{H}^{(0)}$ is tangential to $\vec{a}_2$. u_3 is the coordinate axis normal to the $E^{(0)}$ and $H^{(0)}$ field lines. Equations (6) and (7) can be transformed to the standard transmission line equations by defining a line voltage as the line integral of $E^{(0)}$ from the center conductor to the ground plane, and a line current as the line integral of $H^{(0)}$ around the center conductor. The capacitance C and inductance L per unit length can be computed from the static fields as well.

B. The Quasi-TEM Approximation

By neglecting the longitudinal field components, we have used the same approximation as in the quasi-static approximation of transmission lines with a nonuniform dielectric constant. As suggested by our multiple scales expansion, and as has been shown for uniform transmission lines [15], [16], for low enough frequencies of operation, the z components of E and H fields are small enough to be neglected. A low enough frequency is defined as a frequency that produces a wavelength large compared to the transverse dimensions of the structure, i.e., a small α parameter. We are considering a CPW structure, for which the inner conductor and the gap width do not exceed 200 μm. Since GaAs has a dielectric constant of about 13 and we are working with the impedances of about 50 Ω, frequencies up to approximately 40 GHz will not violate the quasi-static approximation. For higher frequency operation, one could decrease the inner conductor and gap width in order to minimize the radiation loss.

The propagation constant and characteristic impedance of quasi-TEM lines can be expressed as

$$\beta = \omega\sqrt{LC} \tag{8}$$

$$Z_0 = \sqrt{\frac{L}{C}}. \tag{9}$$

Since the phase velocity of a TEM mode is always given by $v_{ph} = c/\sqrt{\epsilon_{\text{eff}}}$, L and C are related by the expression $LC = \mu_0\epsilon_0\epsilon_{\text{eff}}$, and therefore the knowledge of one of them is sufficient to determine all line parameters including the impedance.

Under the qausi-static approximation, an effective dielectric constant is given by $\epsilon_{\text{eff}} = C/C_0$, where C is the capacitance per unit length of the structure, and C_0 is the capacitance per unit length of the structure with air replacing all dielectric materials. The propagation constant of the line can then be written

$$\beta = \frac{\omega}{c}\sqrt{\epsilon_{\text{eff}}} \tag{10}$$

where c is the speed of light in vacuum. The characteristic impedance of the line can be calculated from

$$Z_{\text{TEM}}(z) = \frac{\beta}{\omega C(z)}. \tag{11}$$

In the previous discussion we assumed quasi-TEM propagation, but it can be shown that the generalized transmission line theory holds for non-TEM propagation as well [18], [19].

C. Static Charge Distribution

In the quasi-static approximation, the 2-D potential distribution $V(\boldsymbol{r})$ is related to the charge distribution $\sigma(\boldsymbol{r})$ by

$$V(\boldsymbol{r}) = \int_S G(\boldsymbol{r}, \boldsymbol{r}')\sigma(\boldsymbol{r}')\, d^2 r' \tag{12}$$

where $G(\boldsymbol{r}, \boldsymbol{r}')$ is the static Green's function for the potential due to a charge on the surface S of a semi-infinite dielectric with dielectric constant ϵ_s [20]

$$G(\boldsymbol{r}, \boldsymbol{r}') = \frac{1}{4\pi\epsilon_0\epsilon_{\text{eff}}} \frac{1}{|\boldsymbol{r} - \boldsymbol{r}'|} \tag{13}$$

where

$$\epsilon_{\text{eff}} = \frac{1}{2}(1 + \epsilon_s). \tag{14}$$

The Green's function can be found for many other cases. In case of the finite substrate thickness the Green's function is given by [20]

$$G(\boldsymbol{r}, \boldsymbol{r}') = \frac{\epsilon_s}{\pi\epsilon_0(\epsilon_s + 1)^2} \sum_{n=0}^{\infty} \left(\frac{\epsilon_s - 1}{\epsilon_s + 1}\right)^{2n} \frac{1}{|\boldsymbol{r} - \boldsymbol{r}' - 2nd\boldsymbol{e}_y|} \tag{15}$$

where $\boldsymbol{e}_y$ is a unit vector in y direction and d is the thickness of the substrate. As the Green's function will be eventually represented numerically in the computer program, the only real question as to how it is represented analytically, is how rapidly this analytical representation can be translated to a numerical one (the matrix filling problem). For cases as complicated as those of multiple dielectric layers, it can be shown that extremely efficient matrix filling technique can be developed [23]. It is our belief that such efficient techniques can also be found for Green's function for multiple dielectric layers where the charges may be located away from the interface [24], that is cases involving air bridges, etc.

The total area S can be reduced by noting that far away from the discontinuity the charge distribution will remain essentially unperturbed by the presence of the discontinuity. The charge distribution in these areas can thus be assumed to be known. By dividing the area as shown in Fig. 1, (12) can be written

$$V(x,z) = \int_{-L}^{L} dz' \int_{-W}^{W} dx'\, G(x,x',z,z')\sigma(x',z') + V_{\text{ext}}(x,z) \tag{16}$$

where V_{ext} is the potential in the discontinuity region due to the known charge distribution far away from the discontinuity. $V_{\text{ext}}(x,z)$ can be expressed as

$$\begin{aligned} V_{\text{ext}}(x,z) = &\int_{-\infty}^{\infty} dx'\, G_+(x,x',z)\sigma(x',-L) \\ &+ \int_{-\infty}^{\infty} dx'\, G_-(x,x',z)\sigma(x',L) \\ &+ \int_{-\infty}^{-W} dx'\, G^W(x,x',z)\sigma(x',-L) \\ &+ \int_{W}^{\infty} dx'\, G^W(x,x',z)\sigma(x',-L) \end{aligned} \tag{17}$$

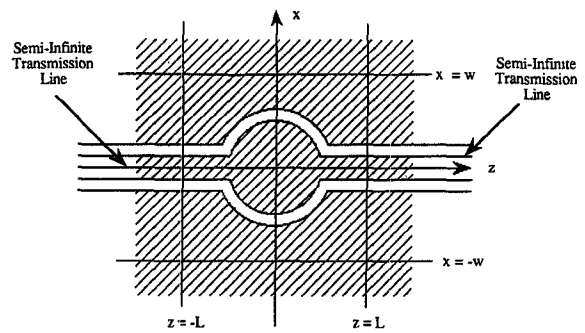

Fig. 1. A coplanar waveguide discontinuity.

where $\sigma(x, \pm L)$ is the charge distribution per unit length on the transmission lines connected to the discontinuity, and $G_\pm$ and G^W are the Green's functions relating the charge distribution in the exterior region to the potential in the interior region $|z| < L$ and $|x| < W$. These functions are given by

$$G_\pm(x,x',z) = \frac{1}{4\pi\epsilon_0\epsilon_{\text{eff}}} \ln\left|(L \pm z) + \sqrt{(L \pm z)^2 + (x - x')^2}\right|^{-1} \tag{18}$$

$$G^W(x,x',z) = \frac{1}{4\pi\epsilon_0\epsilon_{\text{eff}}} \ln\frac{\left|(L - z) + \sqrt{(L - z)^2 + (x - x')^2}\right|}{\left|(L + z) + \sqrt{(L + z)^2 + (x - x')^2}\right|}. \tag{19}$$

In writing [17] we have assumed that the charge distribution for $z \in [-L, L]$ and $|x| > W$ is equal to $\sigma(x, \pm L)$ for $z > 0$ and $z < 0$, respectively. We can now rewrite (16) as

$$V_{\text{int}}(x,z) = \int_{-L}^{L} dz' \int_{-W}^{W} dx'\, G(x,x',z,z')\sigma(x',z') \tag{20}$$

where $V_{\text{int}} = V - V_{\text{ext}}$ is the actual potential on the conductors minus the potential due to the charges in the exterior region. The solution of (20) provides the static charge distribution at the CPW discontinuity. The capacitance per unit length is computed using [17]

$$C(z) = \frac{1}{V} \int_{\text{inner cond.}} |\sigma(x,z)|\, dx \tag{21}$$

where z is the direction of propagation.

III. Numerical Technique

We reduce the integral equation (20) to a matrix equation by using point matching [22]. The motivation for doing point matching is the fact that optical sampling measurements give values for the potential at discrete points. Further, in the case where we wish to find the charge distribution from the known voltage distribution on the electrodes, we can always pick the known voltages to exist at fixed points. We set

$$V'(\boldsymbol{r}) = \sum_n v_n \delta(\boldsymbol{r} - \boldsymbol{r}_n) \tag{22}$$

and expand the charge distribution as

$$\sigma(\boldsymbol{r}) = \sum_n \sigma_n f(\boldsymbol{r} - \boldsymbol{r}_n) \tag{23}$$

where $f(\boldsymbol{r}) = \mathrm{rect}(x/dx)\,\mathrm{rect}(z/dz)$ and dx and dz define the cell size. The resulting matrix equation takes the form

$$[V] = [G][\sigma] \tag{24}$$

where $[\sigma]$ is the unknown vector which contains the solution for the charge density and $[V]$ is the vector which contains the voltages on the electrodes. $[G]$ is the known Green's function matrix with elements

$$G_{n,m} = \begin{cases} G(x_n, x_m, z_n, z_m)\,dx\,dz & m \neq n \\ \frac{dx\,dz}{2\pi\epsilon_0\epsilon_{\mathrm{eff}}} \left\{ \frac{1}{dz} \ln\left(\frac{dz}{dx} + \sqrt{\left(\frac{dz}{dx}\right)^2 + 1} \right) \right. & \\ \left. + \frac{1}{dx} \ln\left(\frac{dx}{dz} + \sqrt{\left(\frac{dx}{dz}\right)^2 + 1} \right) \right\} & m = n\,. \end{cases} \tag{25}$$

The unknown 2-D charge distribution can now be found by simply inverting $G_{n,m}$

$$[\sigma] = [G]^{-1}[V]\,. \tag{26}$$

The matrix inversion can easily be performed using LU decomposition. However, since we are dealing with a 2-D problem the size of the matrix soon becomes very large (an $N \times N$ grid results in an $N^2 \times N^2$ matrix) and large amounts of computer time and storage are needed.

The problem at hand seems very well suited for more efficient iteration techniques [21], [25]. The static charge distribution will often deviate only slightly from a charge distribution composed of 1-D distributions given by the cross-sectional line dimensions at every z coordinate. This distribution can be used as initial value for an iteration technique. In order to solve $[V] = [G][\sigma]$ with a given initial approximation $\sigma^{(0)}$, we used the Gauss–Seidel iterative algorithm with over-relaxation (SOR) [25]

$$\sigma_i^{(k)} = (1-\Omega)\sigma_i^{(k-1)} + \Omega \frac{V_i - \sum_{j=1}^{j=i-1} \sigma_j^{(k-1)} G_{i,j} - \sum_{j=i+1}^{N} \sigma_j^{(k)} G_{i,j}}{G_{i,i}} \tag{27}$$

where the superscript denotes the iteration number and Ω is a relaxation parameter. If $[G]$ is strictly diagonally dominant, then for any choice of $[\sigma^{(0)}]$ this algorithm gives a sequence $\left[\sigma^{(k)}\right]_{k=0}^{\infty}$ that converges to the unique solution of $[G][\sigma] = [V]$ [25]. Overrelaxation parameter values close to 1.5 resulted in rapid convergence for the particular problem considered here.

Since we defined the charge distribution using rectangular functions

$$C(z) = \sum_{\text{inner cond.}} \sigma(x_i, z) \tag{28}$$

and the TEM impedance follows from (11).

IV. Scattering Parameters

With the quasi-static analysis presented above, we have reduced the problem of propagation in a nonuniform CPW structure to a one dimensional problem of TEM propagation on a continuous nonuniform transmission line. The transmission line equations are easily solved using a number of different techniques. They can be transformed to Riccati equations for the reflection and transmission coefficients [26], [27]. Alternatively, they can be transformed to equations for the forward and backward travelling wave variables and then solved using transmission matrices for piecewise uniform transmission lines.

A. The Riccati Equations

By transforming the transmission line equations to Riccati equations, the scattering parameters of the structure can be found by solving the Ricatti equations for the reflection $r(z,f)$ and transmission $t(z,f)$ coefficients [28], [32]

$$\frac{dr(z)}{dz} = -j2\beta(z)r(z) - \left(1 - r(z)^2\right) \frac{dZ_0(z)/dz}{2Z_0(z)} \tag{29}$$

$$\frac{dt(z)}{dz} = -j\beta(z)t(z) + r(z)t(z)\frac{dZ_0(z)/dz}{2Z_0(z)}\,. \tag{30}$$

These equations are solved as initial value problems with initial values $r(-L) = 0$ and $t(-L) = 1$, and integrated from $-L$ to L, to find $S_{11}(f) = r(L,f)$ and $S_{12}(f) = t(L,f)$. The other two matrix elements, S_{22} and S_{21}, can be found by integrating from L to $-L$ with initial values $r(L) = 0$ and $t(L) = 1$.

The Riccati equations are discretized by approximating the equivalent nonuniform line with a piecewise uniform transmission line. For this discrete case the Riccati equations are easily solved by defining the local reflection and transmission coefficients at a point $z = z_{n-1}$

$$\rho_n = \frac{Z_{n-1} - Z_n}{Z_{n-1} + Z_n} \tag{31}$$

$$\tau_n = \frac{2\sqrt{Z_{n-1}Z_n}}{Z_{n-1} + Z_n} \tag{32}$$

where Z_n is the TEM impedance of line section n. The initial value problems are solved according to

$$r_n = \frac{\rho_n + r_{n-1}e^{j2\beta\Delta}}{1 + \rho_n r_{n-1} e^{j2\beta\Delta}} \tag{33}$$

$$t_n = \frac{\tau_n t_{n-1} e^{j\beta\Delta}}{1 + \rho_n r_{n-1} e^{j2\beta\Delta}} \tag{34}$$

where β is given by equation (10) and $\Delta = z_n - z_{n-1}$. Region 0 is connected to a matched load and we, therefore, have the initial values $r_0 = 0$ and $t_0 = 1$. The values for the resulting reflection and transmission coefficients determine the S_{11} and S_{12}, respectively. Similarly, starting the integration from the other port, we can get S_{22} and S_{12}.

B. Transmission Matrix

If the complete S-matrix is needed, it is perhaps easiest to transform the problem to a transmission line network with N

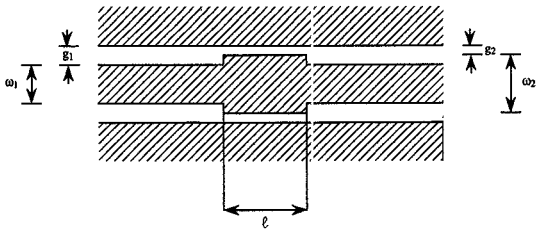

Fig. 2. A CPW test structure, where $g_1 = 86$ μm, $w_1 = 120$ μm, $g_2 = 46$ μm, $w_2 = 200$ μm, and $l = 500$ μm were the dimensions for the measured structure.

cascaded sections, and use the transmission matrix to compute the overall S-matrix. The definition of a T matrix and formulas for conversion to S-parameters and vice verse can be found in the literature [29]. The transmission matrix T_i of the ith section can be written as

$$[T]_i = \frac{1}{\tau_i}\begin{bmatrix} e^{j\beta\Delta} & \rho_i e^{-j\beta\Delta} \\ \rho_i e^{j\beta\Delta} & e^{-j\beta\Delta} \end{bmatrix}. \tag{35}$$

The total transmission matrix is then

$$[T] = \prod_i [T]_i . \tag{36}$$

Using the transformation relationship between S-parameters and T-parameters

$$[S] = \frac{1}{T_{22}}\begin{bmatrix} T_{12} & T_{11}T_{22} - T_{12}T_{21} \\ 1 & -T_{21} \end{bmatrix} \tag{37}$$

the complete S-matrix for the CPW structure can be found. The reference planes are left at the end of the interior region (at $\pm L$), however, they can be shifted by adding the proper phase factors.

V. Application to the Double Step-in-Impedance Discontinuity

The test structure we chose to analyze is the double step-in-impedance, between two 50 Ω coplanar waveguides, shown in Fig. 2. A double step was chosen to have 50 Ω impedance match at the two ports. Using the procedure outlined in the previous sections, we have calculated the charge distribution, local capacitance and impedance, local reflection and transmission coefficients, and the frequency dependent S-parameters for this structure.

The structure was gridded using rectangular cells with $dx = w_1/11$ and $dz = 2\,dx$. This resulted in a total of 858 cells on the connecting lines, and 819 cells on the low impedance line. The static charge distribution was obtained by assuming $V = 1$ V on the center conductor and $V = 0$ V on the ground planes. Fig. 3 shows the 2-D charge distribution. Charge accumulation at the outer corners of the center conductor and charge depletion at the inner corners are evident. It is this perturbed charge distribution close to the junction that gives us the discontinuity parasitics. The charge distribution is perturbed over a finite-length close to the junctions, resulting in frequency-dependent S-parameters.

Fig. 4 shows the computed capacitance and impedance per unit length. We can compare these results with the characteristic impedance of the CPW line without the discontinuity,

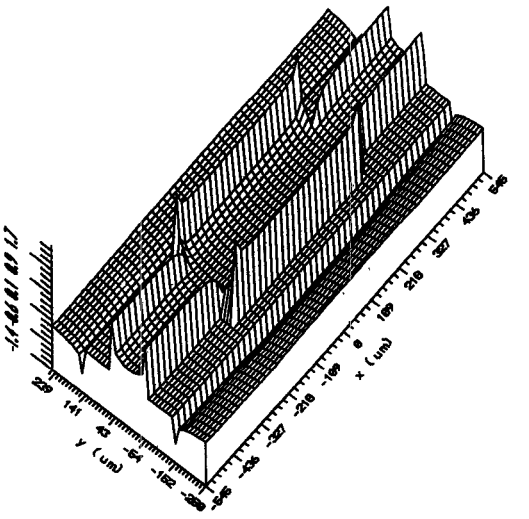

(a)

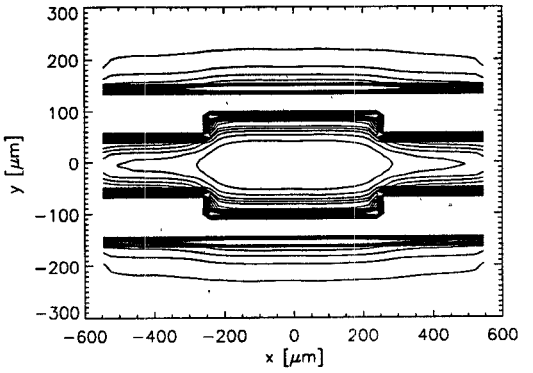

(b)

Fig. 3. Charge distribution: (a) 2-D and (b) contour plots.

using a quasi-static formula from [29]

$$C = \frac{30\pi}{\sqrt{\epsilon_{\text{eff}}}}\frac{K(1/p)}{K\left(\sqrt{1-1/p^2}\right)} \tag{38}$$

where $p = 1 + 2g/w$, g is the width of the gap, w is the width of the inner conductor, and K is the complete elliptic integral of the first kind. For the dimensions given in Fig. 2 the characteristic impedance of the semi-infinite connected lines is 50 Ω, while for the low impedance section of line in between it is 36.6 Ω These are the impedance values from Fig. 4 far from the discontinuity and at $z = 0$.

The solutions of the Riccati equations are shown in Fig. 5. The magnitude and phases of r (excitation from port 2) and t (excitation from port 1) along the line are shown for a frequency of $f = 5$ GHz. The quasi-TEM mode sees a small reflection due to the charge perturbation away from the first junction, and it then experiences a large reflection from the junction. A second large reflection π out of phase is seen at the second junction, nearly cancelling the reflection from the first junction. While this behavior is expected and rather obvious for this particular discontinuity, the solutions of the Riccati equations can provide useful insight for more complicated geometries.

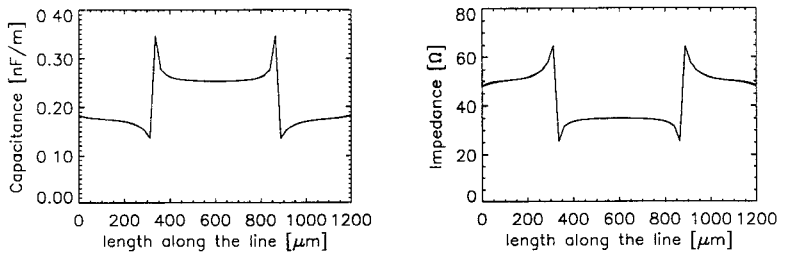

Fig. 4. Capacitance and impedance per unit length along the line.

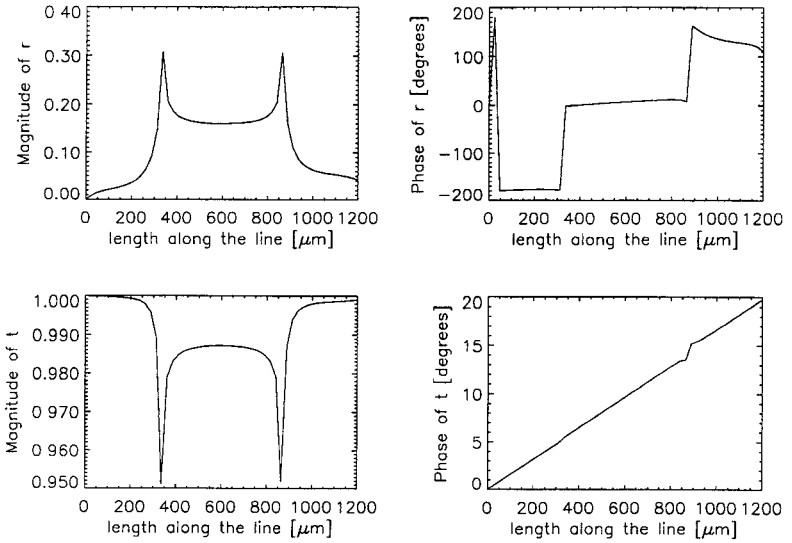

Fig. 5. Magnitude and phase of reflection and transmission coefficient along the line at $f = 5$ GHz.

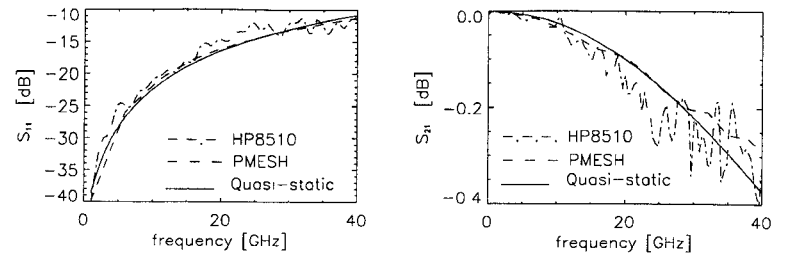

Fig. 6. Magnitude of S_{11} and S_{21} are shown in solid line, PMESH full-wave analysis results are shown with a dashed line and network analyzer measurements are shown in dash dot line.

Fig. 6 shows the computed magnitudes and phases of S_{11} and S_{21} as a function of frequency. For comparison, we have included S_{11} and S_{21} calculated with PMESH, a full wave program developed at the University of Colorado at Boulder [30] and results from measurements performed on the "in-house" fabricated circuit using HP8510 Network Analyzer. In PMESH the electrode gaps are gridded instead of the electrodes. We used two cells per cross-section on the input gap and one cell per cross-section on the interior gap. The total number of cells was 42 in the interior part and 136 on the connecting lines. The comparison is quite good for frequencies less than 30 GHz. The cause of the large deviations at higher frequencies is not understood at this point. Due to the large number of cells used in the static analysis, the total computation time for this case was quite long. However, by examining Fig. 3 (slow variation of σ away from the immediate neighborhood of the junctions) that the number of cells could be drastically reduced without significantly affecting the S-parameter results. Use of symmetry could further reduce the number of cells.

In either technique, quasi-static or full-wave, most of the computation time is used for inverting the Greens function matrix. For the full-wave technique, a matrix inversion is needed for every frequency point. For the quasi-static approach only one matrix inversion is needed, and the time needed to calculate the S-parameters for each additional frequency is negligible. Therefore, with approximately the same number of cells for the two approaches, the computation time for a complete S-matrix frequency plot using the quasi-static approach should be comparable to the time to compute one

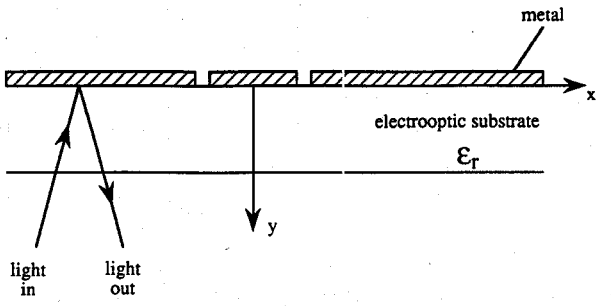

Fig. 7. Optical sampling shown in a transverse cross-section of a CPW line.

frequency point using the full-wave program. Also, the time-domain result can be obtained easily.

VI. Electrooptic Sampling

Direct electrooptic sampling measurements of circuits on GaAs substrates can provide 2-D potential distributions given by

$$V_{eos}(x,z) = \text{const} \cdot \int \vec{E}(x,y,z) \cdot \vec{dl} \qquad (39)$$

where $\vec{dl}$ is tangential to the path of the probe beam. For the configuration shown in Fig. 7, the resulting potential distribution is proportional to the potential difference between the two surfaces. For sufficiently thick substrates, one could assume the bottom surface is an equipotential. For such a case, the line integral of (39) should give the relative spatial (in x and y) variation of the potential distribution on the top surface [31]. The measured potential distribution is therefore identical to within a constant factor, which will be assumed to be zero, to the transmission line voltage defined in the quasi-TEM analysis. These measurements can be used to either directly verify the accuracy of the static potential distributions used in the analysis, or as input to the algorithm and subsequently used to compute transmission line parameters and S-parameters.

Hence, electrooptic sampling measurements of the local quasi-static field distributions combined with the program developed in this paper can provide measurements of the local S-parameters. This technique requires very little real estate and is to a large extent not affected by the unknown terminations of the circuit. This is in stark contrast to conventional techniques of measuring standing wave patterns, which require long line segments ($\approx \lambda/4$) and that the unknown terminations be deembedded. To explore the feasibility of this technique we have taken electrooptic sampling measurements on the structure analyzed in the previous section.

The test structure from Fig. 2 was fabricated on a 400 μm thick GaAs substrate. The circuit was tested using a wafer probe station built for electrooptic probing [13]. Fig. 8(a) shows the measured 2-D potential distribution on a 5×5 μm^2 grid at a frequency of 5 GHz. For comparison, Fig. 8(b) shows the static potential distribution computed from the charge distribution shown in Fig. 3. Besides some local anomalies in the measured result, that can be attributed to surface defects

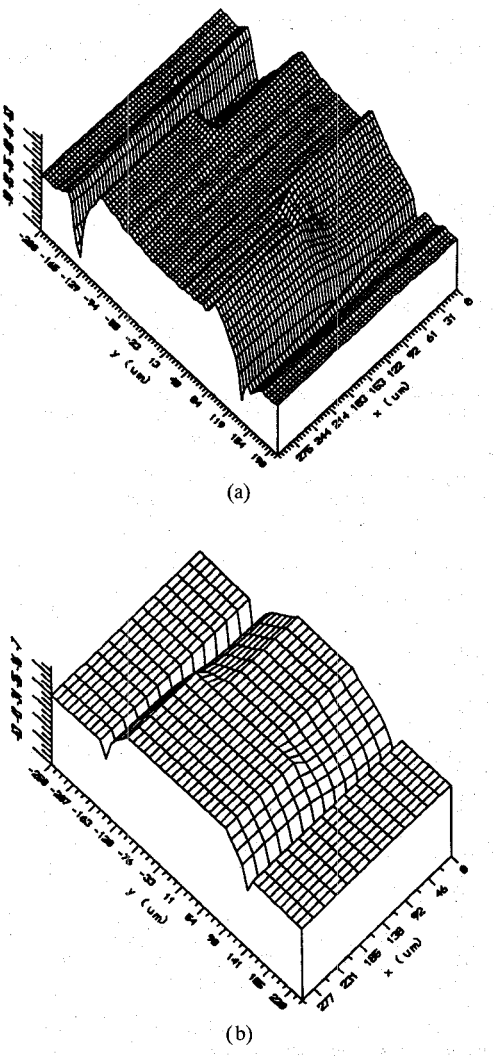

(a)

(b)

Fig. 8. Measured (a) and computed (b) 2-D voltage distribution.

on the wafer, and fewer grid points in the theoretical data, the comparison is quite good.

To check whether we can accurately determine the charge distribution from the measured potential distribution, and therefore compute the equivalent transmission line parameters from the measurements, we first analyzed the 1-D cross-section problem. Fig. 9 shows the measured and computed voltage distribution in one cross-section. The comparison is good, except at the points close to the edges of the center conductor. The large spikes are most likely due to optical diffraction effects at the edges. The slightly negative values on the ground plane can be attributed to the finite substrate thickness [31]. By first eliminating the spikes in the measured potential, we computed the 2-D charge distribution from the measured data. Fig. 10 shows the comparison of the charge distributions, for one cross-section, calculated from the measured and assumed potentials. The small ripples in the measured result are due to fluctuations in the measured conductor potentials. However, it is the total charge on the center conductor that determines the local impedance. Therefore, the accuracy of the "measured" impedance should be sufficient to obtain accurate S-parameter results.

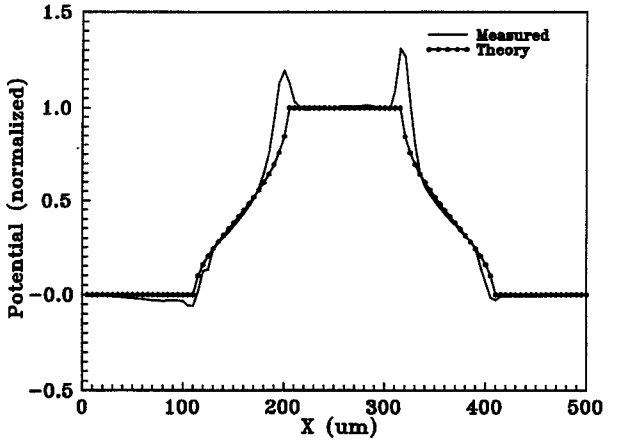

Fig. 9. Comparison of voltage distributions, in a transverse cross section, from measurements and theory.

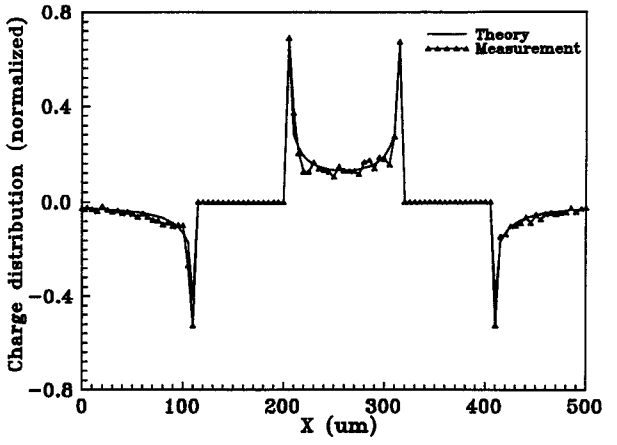

Fig. 10. Comparison of charge distributions, in a transverse cross section, calculated from measured and assumed voltage distributions.

VII. Discussion

In this work, we have applied our method only to two-dimensional discontinuities in two port structures. In this section we wish to discuss some of the straightforward generalizations we plan to implement in the software that will allow us to apply our results to more interesting practical structures.

Clearly, the two port restriction is a serious one. However, the generalization to multiport structures is not a serious implementation problem for the presently discussed technique. The quasi-static solution for the charge distribution can be affected independently of the number of conductors involved. A real problem in implementation is identifying the regions within the circuit which require the full SOR solution as opposed to those in which the simple one dimensional Maxwell solution can be used. This is a practical problem, which exists in the two port case as well. This problem more seriously affects the computer time necessary to converge to a numerical solution than our ability to find a solution. The multiport dynamical solution also becomes more interesting than the two port case. In the multiport, one must identify the multiple paths. The Riccati equation technique is ideal for this purpose. Instead of using the Riccati equation given by (30), one can use coupled Riccati equation given by [33]

$$\frac{d\underline{\underline{F}}(z)}{dz} = i\underline{\underline{\delta}}_F\underline{\underline{F}}(z) + i\underline{\underline{\chi}}_{FB}\underline{\underline{B}}(z) \tag{40}$$

$$-\frac{d\underline{\underline{B}}(z)}{dz} = i\underline{\underline{\delta}}_B\underline{\underline{B}}(z) + i\underline{\underline{\chi}}_{BF}\underline{\underline{F}}(z) \tag{41}$$

where $\boldsymbol{F}$ and $\boldsymbol{B}$ are n forward and backward waves, $\underline{\underline{\delta}}_F$ and $\underline{\underline{\delta}}_B$ are $n \times n$ matrices whose real part denotes phase shift per unit length and whose imaginary part denotes medium gain or loss per unit length, $\underline{\underline{\chi}}_{FB}(\underline{\underline{\chi}}_{FB})$ is $n \times n$ matrix whose elements denote the amount of each backward (forward) wave component to get scattered into each forward (backward) wave component. All of the work presented here assumes an infinite substrate thickness. Green's functions for finite substrate thickness can be found, eg. (15). The finite substrate thickness will have an effect on the charge distribution and capacitance. In most practical cases the line width and substrate thickness will be chosen so as to minimize the field value on the back of the substrate. If the field on the back surface is small, then the finite substrate correction is small. Unlike in microstrip, the substrate thickness does not cause dispersion in CPW lines. CPW lines have a geometrically defined impedance that is not frequency dependent [35]. Although the simple effective dielectric constant formula of (14) no longer applies for the case of a finite substrate, the applicable formula is still nondispersive.

The correction for finite metallization can be also made, as was done in works by the microwave metrology group at NIST [36]. If the metallization exceeds roughly two skin depths, the loss will increase roughly as the square root of the frequency [37]. Such effects can be included "by hand" in such calculations as these presented here. As skin depths are of the order of 0.5 μm for the frequencies of interest here, the finite height of the electrodes will have no dramatic effect on propagation.

Coplanar discontinuities are often 3-D. The most ubiquitous 3-D discontinuity is the airbridge, which must be used in complicated circuits in order to suppress the radiative slot mode in CPW. Many introductory electromagnetics texts [34] solve the problem of the Green's function for a charge above a semi-infinite dielectric. The quasi-static solution in this case will require a three dimensional gridding, but the Riccati equations will still consist of one dimensional coupled equations. Again, generalization poses no fundamental limitation.

A purpose of this work has been to develop the tools necessary to calculate (and subsequently verify) the effects of parasitics on active devices such as MESFETs. Again, in this case, a quasi-static solution can be found by gridding a region that includes the electrodes on the top of the active region and extending out to a point on the coupling lines. To find the charge distribution it is necessary to define voltages on the conductors. The transistor characteristics can be used for this purpose. Iterative use of Riccati equations can be employed to separate parasitics and intrinsic transistor parameters. This is the aim of ongoing work.

VIII. Conclusion

We have presented a new technique for obtaining the frequency dependent scattering parameters of waveguide discontinuities. Using a quasi-static field analysis, the discontinuity is transformed into an equivalent nonuniform transmission line. The scattering parameters are found by analyzing the propagation along this line.

The technique is substantially faster than full-wave techniques. The approximations used are the same as the ones used for the quasi-TEM analysis of uniform nonhomogeneous transmission lines. Therefore, for sufficiently small line dimensions compared to the wavelength, the accuracy should rival that of full-wave techniques. We applied the technique to a double step-in-impedance discontinuity, computing the S-parameters up to 40 GHz. These results compared well to the results from a full-wave analysis of the same structure up to 30 GHz. By combining the technique with the direct electrooptic sampling technique, it is shown that one can obtain local S-parameters from measurement of the local 2-D potential distribution. While we have only considered passive structures here, it is the hope that the technique can be extended to include active devices. This would then provide a technique for finding the parasitic reactances due to the device electrode geometry.

References

[1] M. Goldfarb and A. Platzker, "The effects of electromagnetic coupling on MMIC design," *Microwave and Millimeter Wave CAE,* vol. 1, no. 1, pp. 38–47, Jan. 1991.

[2] J. M. Dunn and L. C. Howard, "An efficient algorithm for the calculation of parasitic coupling between lines in MICs," *IEEE MTT-S Digest,* pp. 405–498, June 1992.

[3] C. M. Snowden and R. R. Pantoja, "GaAs MESFET physical models for process-oriented design," *IEEE Trans. Microwave Theory Tech.,* vol. 40, pp. 1401–1409, July 1992.

[4] F. Filicori, G. Ghione, and C. U. Naldi, "Physics-based electron device modeling and computer-aided MMIC design," *IEEE Trans. Microwave Theory Tech.,* vol. 40, pp. 1333–1352, July 1992.

[5] A. R. Djordjevic, T. K. Sarkar, and Z. Maricevic, "Evaluation of excess inductance of microstrip discontinuity," *Radio Sci.* vol. 26, pp. 565–570, 1991.

[6] R. N. Simons and G. E. Ponchak, "Modeling of some coplanar waveguide discontinuities," *IEEE Trans. Microwave Theory Tech.,* vol. 36, pp. 1796–1803, 1988.

[7] M. Naghed and I. Wolff, "Equivalent capacitances of coplanar waveguide discontinuities and interdigitated capacitors using a three-dimensional finite difference method," *IEEE Trans. Microwave Theory Tech.,* vol. 38, pp. 1808–1815, 1990.

[8] R. Brömme and R. H. Jansen, "Systematic investigation of coplanar waveguide MIC/MMIC structures using a unified strip/slot 3-D electromagnetic simulator," *IEEE MTT Digest,* pp. 1081–1084, 1991.

[9] C. W. Kuo and T. Itoh, "Characterization of shielded coplanar type transmission line junction discontinuities incorporating the finite metallization thickness effect," *IEEE Trans. Microwave Theory Tech.,* vol. 40, pp. 73–80, 1992.

[10] Lord Rayleigh, "On the incidence of aerial and electrical waves upon small obstacles in the form of ellipsoids or elliptic cylinders, and on the passage of electric waves through a circular aperture in a conducting screen," *Phil. Mag,* vol. 44, pp. 28–52, 1897.

[11] J. C. Maxwell, *A Treatise on Electricity and Magnetism,* vol. 1, 3rd ed., (reprint) New York: Dover, 1954, pp. 294–297.

[12] K. J. Weingarten, M. J. W. Rodwell, and D. M. Bloom, "Picosecond optical sampling of GaAs integrated circuits," *IEEE J. Quantum Electron.,* vol. QE-24, pp. 198–220, 1988.

[13] D. R. Hjelme, M. J. Yadlowsky and A. R. Mickelson, "Two-dimensional mapping of the microwave potential on MMICs using electrooptic sampling," *IEEE Trans. Microwave Theory Tech.,* (submitted).

[14] C. C. Lin and L. A. Segel, *Mathematics Applied to Deterministic Problems in the Natural Sciences,* New York: Macmillan, 1974.

[15] G. K. Grünberger, V. Keine, H. H. Meinke, "Longitudinal field components and frequency-dependent phase velocity in the microstrip transmission line," *Electron. Lett.,* vol. 6, pp. 683–685, 1970.

[16] A. F. dos Santos and J. P. Figanier, "The method of series expansion in frequency domain applied to multidielectric transmission lines," *IEEE Trans. Microwave Theory Tech.,* vol. MTT-23, pp. 753–756, 1975.

[17] E. F. Kuester and D. C. Chang, *Theory of Waveguides and Transmission Lines.* University of Colorado, Electromagnetics Laboratory, 1990, Ch. 3.

[18] E. F. Kuester, D. C. Chang, and L. Lewin, "Frequency-dependent definitions of microstrip characteristic impedance," *Digest of Int. URSI Symp. Electromagnetic Waves (Munich),* p. 335, Aug. 26–29, 1980.

[19] J. R. Brews, "Characteristic impedance of microstrip lines," *IEEE Trans. Microwave Theory Tech.,* vol. MTT-35, pp. 30–34, 1987.

[20] W. R. Smythe, *Static and Dynamic Electricity,* 3rd ed. New York: Hemisphere, 1989, pp. 192–194.

[21] W. P. Press, B. P. Flannery, S. A. Teukolsky, and W. T. Vetterling, *Numerical Recipes in Pascal.* Cambridge: Cambridge Univ. 1989.

[22] R. F. Harrington, *Field Computation by Moment Methods.* Malabar, FL: Krieger, 1968.

[23] P. S. Weitzman, J. M. Dunn, and A. R. Mickelson, "An efficient numerical algorithm for the calculation of the electrical properties of coplanar electrodes in the presence of a buffer layer," *J. Quantum Electron.,* (to be published).

[24] M. Kobayashi, "Longitudinal and transverse current distribution on microstrip lines and their closed form expression," *IEEE Trans. Microwave Theory Tech.,* vol. MTT-33, pp. 784–788, 1985.

[25] R. L. Burden and J. D. Faires, *Numerical Analysis.* Boston, MA: PWS-Kent, 1989.

[26] J. R. Pierce, "A note on the transmission line equation in terms of impedance," *Bell Syst. Tech. J.,* vol. 22, pp. 263–265, 1943.

[27] L. R. Walker and N. Wak, "Nonuniform transmission lines and reflection coefficients," *J. Appl. Phys.,* vol. 17, pp. 1043–1045, 1946.

[28] W. C. Chew, *Waves and Fields in Inhomogeneous Media.* Von Nostrand-Reinhold, 1990.

[29] K. C. Gupta, R. Garg, and I. J. Bahl, *Microstrip Lines and Slotlines.* New York: Artech, 1979.

[30] S. Petrakos, "Electromagnetic modeling of coplanar waveguide discontinuities," M.S. thesis, University of Colorado, Boulder, CO, 1991.

[31] J. L. Freeman, D. M. Bloom, S. R. Jefferies, and B. A. Auld, "Accuracy of electrooptic measurements of coplanar waveguide transmission lines," *Appl. Phys. Lett.,* vol. 53, pp. 7–9, 1988.

[32] S. Barkeshli and P. H. Pathak, "On the Diadic-Green's function," *IEEE Trans. Microwave Theory Tech.,* vol. 40, pp. 140–142, Jan. 1992.

[33] D. L. Jaggard, A. R. Mickelson, "Reflection coefficients of almost periodic slabs," Applied Physics, Springer Verlag, 19–4, 405–412, August 1979.

[34] L. C. Shen and J. A. Kong, *Applied Electromagnetism.* Boston, MA: PSW, 1987, pp. 356–358.

[35] E. F. Kuester and D. C. Chang, *Theory of Waveguides and Transmission Lines.* Course Notes for ECEN 5114, Univ. Colorado, Boulder, CO, pp. 93–97, 1991.

[36] R. B. Marks and D. F. Williams, *Characteristic Impedance Determination Using Propagation Constant Measurements.* National Institute of Standards and Technology, Boulder, CO, Mar. 1991.

[37] W. H. Haydl, "Experimentally observed frequency variation of the attenuation of millimeter-wave coplanar transmission lines with thin metallization," *IEEE Microwave Guided Wave Lett.,* vol. 2, no. 8, pp. 322–324, Aug. 1992.

V. Radišić, photograph and biography not available at the time of publication.

Dag R. Hjelme, photograph and biography not available at the time of publication.

Aileen Horrigan, photograph and biography not available at the time of publication.

Zoya Basta Popović, photograph and biography not available at the time of publication.

Alan R. Mickelson, photograph and biography not available at the time of publication.